Measurement of Polarization Observables in $\vec{d}+p\to\vec{p}+p+n$ reaction at $\mathrm{T}_d = 2.0$ GeV

S.L. Belostotski, O.G. Grebenyuk, L.G. Kudin, V.N. Nikulin
St.-Petersburg Nuclear Physics Institute, 188350, Gatchina, Russia

A. Boudard, B. Bonin, M. Garçon, R. M. Lombard, B. Mayer, Y. Terrien
Service de Physique Nucléaire, CEA - Saclay, 91191 Gif-sur-Yvette, France

M. Boivin, E. Tomasi-Gustafsson, J. Yonnet
Laboratoire National Saturne, CEA - Saclay, 91191 Gif-sur-Yvette, France

M. Youn, H.C. Bhang
Department of Physics, Seoul National University, Seoul 151-742, Korea

N.E. Cheung, C.F. Perdrisat
College of William and Mary, Williamsburg, Virginia 23185, U.S.A.

V. Punjabi
Norfolk State University, Norfolk, Virginia 23504, U.S.A.

J. Erő[†], Z. Fodor, P. Koncz, Z. Seres
KFKI Research Institute for Particle and Nuclear Physics, 1525 Budapest, Hungary

(January 13, 1998)

We have studied the deuteron breakup in the $p(d, 2p)n$ reaction at T$_d$=2.0 GeV. In this experiment, the vector analyzing power A_Y, the tensor analyzing power A_{YY}, and the polarization of the forward scattered proton are measured close to the quasi free pp scattering kinematics. These observables are presented as a function of the neutron momentum ranging from 0.04 to 0.45 GeV/c in the rest frame of the deuteron. Marked deviations from the Impulse Approximation using conventional deuteron wave functions are observed. Corrections due to the multiple scattering, the final state interaction and the Δ excitation are calculated in a model where the spin-isospin structure of the elementary amplitudes is treated rigorously. With this model, a reasonable account of the measured polarization observables is obtained. The global agreement with all observables is however not good enough that we can reliably discriminate between conventional wave functions.

† Prof, J. Erő died on Jan. 2, 1997, before this paper could be published. We wish to remember him as a very kind person, one who was very interested in this physics and an inspiration to all who knew him.

I. INTRODUCTION

The deuteron is a very interesting nucleus as a pure correlation between the proton and the neutron. A detailed study of its structure will bring information on the strong interaction between two bound nucleons in specific quantum states.

While the static properties of the deuteron, like binding energy, radius, magnetic and quadrupole electric moments, are well known, the dynamics of this system are less well documented. The knowledge of the probability for a nucleon to have an internal momentum q in the deuteron is a strong constraint for the NN potential. The larger this momentum, the smaller the relative distance between the two nucleons.

As the inter-nucleon distance decreases, meson exchange, and excitation of the nucleon internal structure leading to NN^* and $\Delta\Delta$ components and even new dynamical effects appear. These ultimate effects still under investigation are due to the increasing overlap between the two nucleon's three-quark bags. Experimental information from the polarization observables as functions of q, is sensitive to small components of the wave function and so could help to disentangle these effects.

The kinematics of the exclusive process $\vec{d} + p \to \vec{p} + p + n$ is completely specified for each identified event, and scanning in q is possible assuming the validity of Plane Wave Impulse Approximation (PWIA). A measurement of the vector and tensor analyzing power and of polarization transfer to one outgoing proton, provides 4 independent observables of the reaction in addition to existing cross-section data. This redundancy will be a stringent test for a good understanding of the reaction mechanism. Experimentally the analyzing powers are ratios of cross sections and offer easy access to small probabilities with regards to normalization and efficiency problems.

The usefulness of polarized–deuteron breakup experiments was emphasized and studied in several papers [1–3].

The PWIA for the reaction $p(d, 2p)n$ under investigation assumes that one of the nucleons in the deuteron is a spectator, being unaffected by the breakup process. The momentum of this nucleon in the outgoing channel boosted to the deuteron rest frame is interpreted as its fermi momentum q or internal momentum of the nucleon in the deuteron. Hence, in the framework of the IA, it is possible to study the internal momentum distribution $|\Phi(q)|^2{=}u^2(q) + w^2(q)$. Within the same approximation, the polarization observables are sensitive to the ratio $u(q)/w(q)$, momentum space wave functions of the S and D state components of the deuteron, respectively.

The structure of the deuteron has been the subject of many investigations, both theoretically and experimentaly.

Conventional theoretical studies are based on models of the N-N potential. From the potential, the wave function of the deuteron as a bound state of the proton and the neutron is deduced. Among the numerous results, we will specifically use the Bonn wave function [4] and the Paris wave function [5] as representatives of reasonable variations of various phenomenological potentials.

A number of ed elastic scattering experiments have been performed to measure the charge, quadrupole and magnetic form factors ([6] and references included therein) up to a transfered momentum of $4.6 fm^{-1}$. However the transverse and longitudinal structure functions, $A(Q^2)$ and $B(Q^2)$ have been measured up to $8 fm^{-1}$ and $10 fm^{-1}$, respectively. It should be noted that if the momentum transfer in elastic scattering is Q, then the corresponding value of the deuteron internal momentum is $q = Q/2$.

Exclusive and inclusive deuteron break up reactions, both providing in principle direct access to the deuteron wave function have been extensively investigated. There are data from the exclusive d(p,2p)n [7–15] and d(e,e'p)n [16–18] reactions, and also from the inclusive reaction A(d,p)X [19–22]. An exclusive experiment on polarized deuteron photodisintegration is in progress in Novosibirsk [23] and at NIKHEF [24].

Inclusive polarized deuteron breakup has been intensively investigated using Dubna and Saturne polarized deuteron beams [21,22,25–28]. These studies have demonstrated that polarization observables like the tensor analyzing power T_{20}, were independent of beam energy, and only weakly dependent upon the target nature, when analyzed as a function of internal momentum q, over a range of deuteron energies from 1.25 to 4.4 GeV. Polarization transfer data show a similar energy and target independence as T_{20}, although the experimental evidence is weaker.

The various reactions give a coherent picture of the deuteron density and are well understood in terms of the IA with a conventional deuteron wave function up to momentum of about 200 MeV/c. Above this q value, depending upon the reaction and the kinematics, the results differ significantly. After corrections to the PWIA, the $|\Phi(q)|^2$ from (e,e'p) experiment [18] is in agreement with the Paris wave function up to 500 MeV/c, while the $|\Phi(q)|^2$ extracted from (p,2p) [15] agrees better with the Bonn wave function in the same internal momentum range. In inclusive breakup, with a proton detected in the forward direction, a marked bump or excess of probability, is observed around 320-350 MeV/c in the data, above conventional wave function predictions for all targets and energies of the deuteron beam [19–22]. Up to now this bump is not unambiguously understood.

New degrees of freedom in the deuteron structure were also suggested; for example, Kerman and Kisslinger (followed by others) introduced $\Delta\Delta$ and NN^* isobaric components in the deuteron wave function [29]; Ableev et al. [20] suggested 6-quark effects following many theoretical studies [30–32].

Whatever the deuteron structure, the PWIA needs to be complemented at high internal momenta by known effects like Final State Rescattering (FSR). The off-shell effect of the proton in the reaction d(e,e'p) was discussed in ref. [18]. The estimated correction to the cross section was found to be small (a few percent). The possibility of FSR processes was studied [1,8] and included in most of the interpretations. This aspect is especially detailed in [33] where the exclusive $d(p,2p)n$ and inclusive $p(\vec{d},p)X$ cross section and tensor analyzing power T_{20} are computed up to double scattering but in a coplanar geometry. The virtual Δ excitation was also discussed [34,10], for the d(p,2p)n cross section, concluding that it can be dominant when the two final protons are emitted symmetrically with an invariant mass around $M_N + M_\Delta$. In other kinematics closer to the quasi free scattering, the virtual Δ contribution was shown [15] to have modest effects.

When FSR or Δ excitation play a significant role, it is not possible to interpret the momentum of the spectator nucleon as the internal momentum of the deuteron constituent nucleons. Yet this interpretation still provides an easy way to picture and discuss experimental results which are five-fold differential in a 3 body final state experiment. We expect that polarization data will provide a test of the validity range of the PWIA from the universality of observables with respect to q, as well as a strong constraint in the separation of the reaction mechanism from possible unconventional deuteron components.

In the present experiment the tensor A_{YY} and vector A_Y analyzing powers, and the polarization of the outgoing fast proton in the $\vec{d} + p \to \vec{p} + p + n$ exclusive reaction, have been measured with polarized deuteron beams from the SATURNE synchrotron at Laboratoire National Saturne in France. The coincidence cross sections measured in the same experiment were published [35] and are thus not discussed in the present paper.

The theoretical model used for the analysis of the polarization observables is similar to the one used for the Gatchina unpolarized $pd \to ppn$ experiment [15]. More details concerning the description of polarized observables are given in section II. The experiment and data reduction are described in section III. In section IV, the results are presented and discussed with a summary of the theoretical model used. The conclusions are drawn in section V.

II. DESCRIPTION OF OBSERVABLES

In the PWIA, first order approximation for the reaction mechanism, the spectator nucleon remains in the same spin state and has the same momentum as prior to the reaction.

In this experiment the angles of detection for the two protons were chosen to favor quasi free pp-scattering events, leaving the neutron in the deuteron as a spectator.

The amplitude of the reaction in the PWIA can be written as

$$F^{\mu_1,\mu_2,\mu_3}_{M,\mu} = \langle \chi^{\mu_1}_{1/2}, \chi^{\mu_2}_{1/2}, \chi^{\mu_3}_{1/2}, |\mathrm{V}_{pp}(1,2)| \chi^{\mu}_{1/2}, \Psi^M_1(1,3,\vec{q}) \rangle, \tag{1}$$

where the spin part of the wave functions is specified with a notation illustrated in Fig 1.

The deuteron wave function in momentum space is

$$\Psi^M_1(1,3,\vec{q}) = \frac{1}{q} \sum_{L=0,2} u_L(q) [Y_L(\hat{q}).\chi_1(1,3)]^M_1, \tag{2}$$

where the spherical harmonics $Y_L(\hat{q})$ determine the angular dependence, and χ_1 is the deuteron spinor. The radial dependence of the S and D state of the deuteron are the functions $u_L(q)$ to be denoted in the following as $u(q)$ and $w(q)$, or u and w for short.

The cross section of the exclusive reaction for a given spin state M of the initial deuteron is then

$$\frac{d^5\sigma_M}{dp_1 d\Omega_1 d\Omega_2} = d\sigma_M = \frac{1}{2}\sum_{\mu}\sum_{\mu_1,\mu_2,\mu_3} |F_{M,\mu}^{\mu_1,\mu_2,\mu_3}|^2, \tag{3}$$

where the notation $d\sigma_M$ is introduced for shortness.

Following the Madison convention [36] the differential cross section for vector (p_y) and tensor (p_{yy}) polarization of the deuteron beam is

$$\frac{d^5\sigma}{dp_1 d\Omega_1 d\Omega_2}(p_y, p_{yy}) = \frac{d^5\sigma}{dp_1 d\Omega_1 d\Omega_2}(0,0)\left[1 + \frac{3}{2}A_Y p_y + \frac{1}{2}A_{YY} p_{yy}\right], \tag{4}$$

with corresponding vector and tensor analyzing powers defined as

$$A_Y = \frac{d\sigma_{M1} - d\sigma_{M-1}}{d\sigma_{M1} + d\sigma_{M0} + d\sigma_{M-1}}, \tag{5}$$

$$A_{YY} = \frac{d\sigma_{M1} + d\sigma_{M-1} - 2d\sigma_{M0}}{d\sigma_{M1} + d\sigma_{M0} + d\sigma_{M-1}}, \tag{6}$$

and the unpolarized cross section as

$$\frac{d^5\sigma}{dp_1 d\Omega_1 d\Omega_2}(0,0) = d\sigma = \frac{d\sigma_{M1} + d\sigma_{M0} + d\sigma_{M-1}}{3}. \tag{7}$$

From these expressions, one can derive the following expressions for the three observables in the PWIA:

$$A_Y(q) = P_{pp}\left[\frac{2(u^2 - w^2) - uw\sqrt{2}}{3(u^2 + w^2)}n^y + \frac{w(\sqrt{2}u + w)}{u^2 + w^2}k^y(\vec{k}, \vec{n})\right] = P_{pp}B_Y, \tag{8}$$

$$A_{YY}(q) = \frac{1}{2}\left(3\hat{q_Y}^2 - 1\right)\frac{w(2\sqrt{2}u - w)}{u^2 + w^2}, \tag{9}$$

$$d\sigma = \frac{d\sigma_{pp}}{4\pi q^2}(u^2 + w^2), \tag{10}$$

where $\vec{k} = \vec{q}/q = \vec{\hat{q}}$, $\vec{n}$ is the unit vector along the normal to the plane of the pp scattering, P_{pp} the polarization, and $d\sigma_{pp}$ the differential cross section of the pp scattering. The expression for $A_Y(q)$ defines a structure function $B_Y(q)$ for the deuteron.

The polarization of the fast proton, which was also measured in this experiment, is defined as

$$P = \frac{N_{up} - N_{down}}{N_{up} + N_{down}} \tag{11}$$

where the number of fast protons in the up or down spin state is:

$$N_{up(down)} = \sum_M n_M d\sigma_M^{up(down)} = \sum_M n_M \frac{1}{2}\sum_{\mu,\mu_2,\mu_3} |F_{M,\mu}^{up(down),\mu_2,\mu_3}|^2. \tag{12}$$

If the proportion of incident deuterons in each spin state is n_+, n_- and n_0, then the vector and tensor polarization of the beam are:

$$p_y = n_+ - n_- \tag{13}$$

$$p_{yy} = n_+ + n_- - 2n_0 \tag{14}$$

$$n_+ + n_- + n_0 = 1 \tag{15}$$

and the spin structure of the $p(d,2p)n$ amplitude leads in IA to:

$$P = \frac{P_{pp} + 3B_Y D_{pp} p_y/2 + A_{YY} p_{yy} P_{pp}/2}{1 + 3A_Y p_y/2 + A_{YY} p_{yy}/2} \tag{16}$$

where D_{pp} is the depolarization parameter in free pp scattering. The depolarization parameter for the $p(d,2p)n$ reaction can be defined as

$$D_v = \frac{d\sigma^{\uparrow\uparrow} - d\sigma^{\uparrow\downarrow}}{3d\sigma}, \tag{17}$$

with

$$d\sigma^{\uparrow\uparrow} = \frac{1}{2} \sum_{\mu,\mu_2,\mu_3} \left[|F_{1,\mu}^{\uparrow,\mu_2,\mu_3}|^2 + |F_{-1,\mu}^{\downarrow,\mu_2,\mu_3}|^2 \right], \tag{18}$$

$$d\sigma^{\uparrow\downarrow} = \frac{1}{2} \sum_{\mu,\mu_2,\mu_3} \left[|F_{-1,\mu}^{\uparrow,\mu_2,\mu_3}|^2 + |F_{1,\mu}^{\downarrow,\mu_2,\mu_3}|^2 \right], \tag{19}$$

and

$$d\sigma = \frac{1}{2}\frac{1}{3} \sum_{M,\mu,\mu_1,\mu_2,\mu_3} |F_{M,\mu}^{\mu_1,\mu_2,\mu_3}|^2. \tag{20}$$

The D_v observable measures the fraction of fast protons with their spin in the same direction as the deuteron spin. In the IA, this observable is equal to

$$D_v = B_Y D_{pp}, \tag{21}$$

where B_Y is the same deuteron structure function which was introduced earlier in the definition of A_Y; B_Y has values in the range from $+1$ to -1.

Labelling the polarization of the fast proton P^+ for an incident deuteron in the state $(M = +1)$, and P^- for the state $(M = -1)$, follows the expression of D_v:

$$D_v = \frac{P^+ - P^-}{3p_y} + A_Y \left(\frac{P^+ + P^-}{2} \right). \tag{22}$$

Combining the two independent quantities P^+ and P^- it can be shown that

$$P_0 = \frac{P^+ + P^-}{2} + \frac{3}{2} A_Y p_y \left(\frac{P^+ - P^-}{2} \right), \tag{23}$$

which is the polarization of the fast proton for unpolarized deuteron beam. In the IA it is equal to the polarization in free pp scattering.

$$P_0 = P_{pp}. \tag{24}$$

To summarize, we note that the spin observables A_Y, A_{YY} and D_v are functions of the ratio between the S and the D states at an internal momentum $\vec{q}$ fixed by the kinematics in the outgoing channel. In the IA, the momentum $\vec{q}$ is the momentum of the spectator neutron, in the deuteron rest frame. In this paper all the observables are shown as functions of $|\vec{q}|$, being summed up over other kinematic variables within the experimental acceptance. This representation of observables which are 5-fold differential, does display the main dynamical features of the reaction to first order; this point will be further discussed in more detail in sect. IV.

At large values of $|\vec{q}|$, the IA should be complemented with other graphs including FSI, Δ excitation and so on (see Fig 2), which modify the observables substantially. It follows that strong constraints for the calculation of the reaction mechanism will result from the comparison of theoretical predictions with the four independent observables A_Y, A_{YY}, D_v and P_0.

The term $\hat{q}_Y$ in eq (9) takes into account events with pp scattering out of the horizontal plane resulting from the large vertical aperture of the detectors in this experiment. But the P_{pp} and D_{pp} parameters are defined only for coplanar pp scattering.

Expressions for the analyzing power, valid in the framework of the IA, and similar to eq (8) and eq (9,) have been discussed by C.Wilkin [37], and used for analysis of inclusive deuteron breakup reaction data [21,22] and of ^{6}Li inclusive breakup reaction data [38]. However, eq (8) and eq (9) differ from them by the fact that they contain a term depending on q_Y.

III. DESCRIPTION OF EXPERIMENT AND DATA HANDLING

The polarized deuteron beam from the atomic ion source HYPERION is injected in the pre-accelerator MIMAS and then into the synchrotron ring SATURNE, where it is accelerated up to 2 GeV. The extracted beam is transported to the target point of the SPES 4 spectrometer shown in Fig 3 [39]. The scattering angle θ_1 of the fast proton p_1 was set to 18.3° by means of a movable dipole magnet upstream of the target. The recoil proton p_2 was detected in coincidence with the proton p_1 within a range of scattering angles θ_2 from 52.5° to 61.5° with the Recoil Spectrometer (RS) located in the target area. The beam was stopped downstream from the target in a beam dump . The RS detectors were protected from a direct view of the beam dump by a concrete wall of 1.5 m thickness.

A. The deuteron beam and the target.

The beam was focused on the target with a spot of dimensions 6 mm horizontally by 2.2 mm vertically. The target was a vertical cylinder cell filled with liquid hydrogen. The cell had a diameter of 40 mm with walls made of 150 μm thick mylar. The slow recoiling protons exited the target vacuum chamber 38 cm away from the target cell through a 50 μm titanium window.

The beam time structure was of 0.4 s duration at 3 s repetition period. The beam intensity was limited to 3.0×10^9 deuterons per spill to maintain acceptable values of the leakage current in the proportional chambers of RS located close to the target. Also when data were taken close to the quasi elastic peak the beam intensity was further reduced to keep the dead time of the data acquisition system reasonably small.

There is no depolarization of the deuterons during the acceleration in SATURNE [40], so that the polarization can be measured at 385 keV, with a low energy polarimeter [41] located at the exit of the ion source before injection into the pre-accelerator MIMAS. The polarization state of successive beam bursts was repeated cyclicly, either in the two-state mode (states 2 and 3), or in the four-states mode (states 5,6,7 and 8). Successive beam bursts had a different polarization, as summarized in Table I, together with the maximum polarization delivered by the atomic source in each one of these states.

The data were obtained during two separate periods in two consecutive years. The measured polarizations were constant during each period and are given in Table II after appropriate normalization [41] and dead time correction [42]. In addition to the statistical uncertainty from the beam polarization measurements, the estimate of the systematic error is ±6% for the tensor and ±4% for the vector polarization [41]. The data measured during the two runs have been summed after checking that they were consistent within statistical uncertainty.

B. The SPES 4 spectrometer.

The spectrometer SPES 4 is shown in Fig 3; its configuration is discussed in detail in [39,43]. A time of flight is obtained with the start from scintillators (1 mm thickness) at the intermediate focus (IF), and the stop given by scintillators (3 mm thick) in the final focus (FF) (Fig 4); the time-of-flight has a base distance of 16.8 m and provides excellent trigger selectivity for protons. The spectrometer momentum resolution is $\Delta p/p \sim 10^{-3}$. A collimator defined a solid angle of $\Delta\Omega = 0.69$ msr, with angular acceptances $\Delta\theta_h = 1.04°$ horizontally, and $\Delta\theta_v = 2.17°$ vertically; the momentum acceptance was 4% without cuts, extending to 6% with a decreasing solid angle. The angular resolution after analysis of the tracks was $\sim 0.1°$ (FWHM) horizontally and $\sim 0.2°$ vertically. The polarization of the protons p_1 selected by SPES 4 is measured with the polarimeter POMME [44]. The polarimeter (Fig 4) measures the azimuthal asymmetry of p-C inclusive scattering from a 31.2 cm thick carbon analyzer located near the FF plane. Proton tracks upstream and downstream of the carbon block are reconstructed using 6 multi-wire (XY) proportional chambers with sensitive area 50×50 cm^2 for the 3 front chambers and 100×100 cm^2 for the 3 rear chambers. The polarimeter has its own trigger given by a coincidence between the FF, P and Q scintillators. The three front chambers are also used for the precise tracking that determines the momentum and scattering angle at the primary liquid hydrogen target.

C. The "Recoil Spectrometer" RS.

The "Recoil Spectrometer" consists of two X,Y modules of multi-wire proportional chambers CH1 and CH2, an array of 7 scintillation plates ΔE_i and a 7×4 matrix of scintillation blocks E_{ij} for $\Delta E, E$ analysis (Fig 5).

The distances between the target point and the wire chambers are respectively 1.2 m and 2.7 m, which together with the 4 mm spacing of the wires and the multiple scattering in the target and the titanium window result a resolution $\Delta\theta_2 \sim 0.45°$ (FWHM). The seven plates of the ΔE array, each of $500 \times 125 \times 10$ mm^3 , were placed horizontally at a distance of 3.03 m from the target. Each plate is viewed on both sides by a photomultiplier, and for each of them a time and a energy loss information are recorded. The E matrix consists of 28 blocks plastic scintillator $120 \times 120 \times 200$ mm^3, each of them viewed by a single photomultiplier and with a charge information recorded.

D. Calibration by elastic dp scattering.

To obtain an absolute calibration of the angle between SPES 4 and RS, elastic two body scattering $dp \to pd$ data were recorded and analyzed for several SPES 4 angles, θ_{SPES4} of +7.0°, +6.5° and –7.0°. In this calibration, the deuteron was detected in SPES 4, and the proton in RS. The measurement was extended to negative angle in order to have a constraint for the determination of the 0° value of θ_{SPES4}; it was found that the nominal zero angle was shifted by 0.33° (to the left, the usual scattering side in a SPES 4 experiment).

For the larger θ_{SPES4} values of 7.9°, 9.54°, 10.93°, and 12.86°, the correlation of the elastic scattering data and the 2-body kinematics constraint is shown in Fig 6. The values $\Delta\theta_d$ and $\Delta\theta_p$ are the direct angular measurement in SPES-4 and RS with respect to their central axis. From a comparison between the experimental points and the curve, it was determined that the angle between the axis of SPES 4 and RS was 75.0°.

The elastic scattering data were also used to calibrate the time of flight and the ΔE and E detectors of the RS for known proton energies.

A more detailed description of all these calibrations can be found in ref. [45].

E. Event selection.

The $p(d, 2p)n$ reaction events were selected by requiring the appropriate timing between SPES 4 and RS (rTOF). The accuracy for rTOF was better than 1.0 ns (FWHM). Once the proton in SPES 4 was identified and its momentum $\vec{p}_1$ reconstructed, rTOF could be converted to the time of flight of the recoil proton, from the target vertex to the ΔE detector. We denote this converted time of flight as TOF. This value represents the particle velocity detected by RS allowing to calculate the recoil proton momentum p_2. The $(\Delta E, p_2)$ scatter plot was used to identify protons. The momentum p_2 was used instead of the measured energy in the E_{ij} counters, because above 175 MeV, the protons were not stopping in the 200 mm thick plastic scintillators. This additional information E_{ij} was only used to solve ambiguous cases.

For the $dp \to p_1p_2n$ process at a given deuteron kinetic energy T_d, when $\vec{p}_1$ is determined from the SPES 4 measurement and ϕ_2 from the RS measurement, there is a correlation

$$f(T_d; \vec{p}_1, \phi_2, p_2, \theta_2) = 0 \tag{25}$$

between p_2 and θ_2. This equation defines a maximum scattering angle $\theta_2^{max}(\vec{p}_1, \phi_2)$ and two possible values of p_2 for a given scattering angle θ_2 smaller than this maximum. In the following, the low energy solution (LES) corresponds to the lowest value of p_2 and the high energy solution (HES) to the highest. The correlation is used to select the $dp \to ppn$ process from the remaining background. The angle θ_2 is measured by the MWPC of RS and p_2 by the TOF, assuming the RS particle to be a proton.

Due to multiple scattering and detection resolutions, the detected events are spread around the pure kinematical correlation (25), even outside the kinematical limit. To overcome this difficulty, a method that minimizes the probability of deviation from the three body kinematics was used. A "distance" d between the measured event at (θ_2^m, p_2^m) and the expected (θ_2, p_2) correlation is defined:

$$d^2 = \frac{(p_2^m - p_2)^2}{\sigma_{p_2}^2} + \frac{(\theta_2^m - \theta_2)^2}{\sigma_{\theta_2}^2} \tag{26}$$

where θ_2 is actually given by:

$$\theta_2 = g(\vec{p}_1, \phi_2, p_2) \tag{27}$$

derived from the correlation f. The closest value (θ_2^c, p_2^c) is obtained by a minimization of expression (26) with respect to p_2.

This value (θ_2^c, p_2^c) will then determine all other kinematical quantities associated with the measured event and compatible with the $dp \to ppn$ three body kinematics. A cut is also applied on the minimized d^2 value (smaller than 4) to select the $dp \to ppn$ reaction and reject background.

The background contamination was determined from Fig 7 in a region outside the kinematic limits of the $dp \to ppn$ reaction. In the figure, the contour which is equivalent to the allowed phase space of $dp \to ppn$ reaction is shown, but shifted to larger value of TOF. The estimated background was around 2% in total, but it affected mostly the region of low counting rate (e.g. large q). In Fig 8, the estimated background and real $p(d, 2p)n$ events after subtraction of the background, are shown as a function of q.

For the selected events with $\vec{p}_1$ and $\vec{p}_2$ determined, the magnitude of the spectator momentum q was calculated with a typical accuracy of 8 MeV/c (r.m.s.). For a given setting, the precision on q ranges from 2 MeV/c to 30 MeV/c in extreme cases.

The measurements were performed at six different settings of the magnetic fields in SPES 4 with central values of 1.6, 1.7, 1.8, 1.9, 2.0 and 2.05 GeV/c, corresponding to the different domains of q listed in Table III.

F. Data handling for the polarization of the fast proton.

Only for those events identified as originating from the $dp \to ppn$ reaction was the polarimeter POMME information analyzed. The particle trajectories reconstructed before and after the scattering, and the reaction vertex in the graphite analyzer were obtained from the front and rear chambers coordinates (Fig 4). The thickness of the analyzer was 31.2 cm. A cut on the range of the reaction vertex to match the actual size of the ^{12}C block was first applied. The distribution of the θ_c scattering angle after this cut is shown in Fig 9 (a).

Because the small scattering angles are mostly due to multiple scattering and not to a nuclear interaction, events with $\theta_c < 2.5°$ were rejected. These events have negligible asymmetry and suffer from a bad determination of the azimuthal angle (φ_c). A "cone test" [46] was then applied. This test requires that the cone defined by θ_c for the running event lies within the acceptance of the polarimeter to consider this event. It is used to eliminate systematic asymmetries by ensuring a sufficient azimuthal acceptance. The efficiency of the polarimeter for this experiment was typically 8%.

The azimuthal angle (φ_c) distribution of the events after the cone test is shown in Fig 9 (b). A φ_c distribution was obtained for a number of q-values. To get reasonable statistics, the binning size for q was taken as 0.05 GeV/c.

For each event, the coefficients

$$a_1 = A_y^c(\theta_c)\cos(\varphi_c) \tag{28}$$

$$a_2 = (A_y^c(\theta_c))^2 \tag{29}$$

were calculated with $A_y^c(\theta_c)$ the analyzing power of the inclusive $p+^{12}C$ reaction at the scattering angle (θ_c). Values of $A_y^c(\theta_c)$ were obtained in a previous calibration of the POMME polarimeter [44]. For each bin of q, the quantities a_1 and a_2 were summed for all events, and the proton polarization was obtained as

$$P^{\pm}(q) = 2\frac{\sum a_1(q)}{\sum a_2(q)}. \tag{30}$$

This polarization P^+ (P^-) is measured for the polarization state 2 (respectively 3) of the incident deuteron beam.

Relations (22) and (23) were used to calcute the observables.

The statistical uncertainty on P_0 and D_v is rather large. In Fig 10 each observable obtained for different SPES 4 momentum is plotted as a function of q but separately for the high and the low energy solution of the proton. With this partition, q seems a good variable at least to the level of accuracy of the experiment as verified by a χ^2 test between measurements at the same q value. Most of the χ^2 per point are much smaller than 1. So values obtained at the same q but for different SPES 4 settings were combined.

The internal momentum q is the scaling variable only below $\sim 200 MeV/c$, where the IA is known to be valid. Above this value, the deviation from the IA for P_0 and D_v should be smaller than the precision of the measurement. There is however an obvious difference between the high and the low energy solution. They correspond to different orientations of the neutron momentum $\vec{q}$ which should induce very different corrections to the IA and this is the reason why we have kept this dependence.

G. Observables from selected events

As was mentioned in previous sections, there are two kinematical solutions and the observables A_Y, A_{YY}, P_0, and D_v can be calculated as a function of q for each solution separately. Denoting the number of selected events after background subtraction as $N_i(q)$, where i is the beam polarization state number given in Table I, the analyzing powers A_Y and A_{YY} are given by:

$$\begin{aligned} A_Y(q) &= -\frac{2}{3} \times \frac{1}{|p_y|} \frac{N_2(q) - N_3(q)}{N_2(q) + N_3(q)}, \\ A_Y(q) &= \frac{2}{3} \times \frac{1}{|p_y|} \frac{N_5(q) - N_6(q) + N_7(q) - N_8(q)}{N_5(q) + N_6(q) + N_7(q) + N_8(q)}, \\ A_{YY}(q) &= 2 \times \frac{1}{|p_{yy}|} \frac{N_5(q) + N_6(q) - N_7(q) - N_8(q)}{N_5(q) + N_6(q) + N_7(q) + N_8(q)}, \end{aligned} \tag{31}$$

where the beam polarizations p_y and p_{yy} are defined in eq (13), eq (14) and in Table II. Expressions (31) follow from eq (4), eq (5) and eq (6). The complet set of experimental values with statistical errors is given in Table IV (high energy) and Table V (low energy of the recoil proton p_2).

IV. THEORETICAL INTERPRETATION AND DISCUSSION OF RESULTS

A. Model used

The kinematics of this experiment is dominated by the p-p quasi elastic scattering. Nevertheless, the n-p term taking into account scattering of the neuteron in the deuteron off the target proton producing either the slow recoil proton (p_2) detected with RS or the fast one (p_1) detected by the forward spectrometer SPES-4 was added coherently to the main p-p scattering term in the IA. This n-p contribution to the cross section is rather small but it is not negligible for the polarized observables.

All the NN second order rescattering terms (FSR) were included taking into account both low energy final state interaction and Glauber type rescattering of the fast protons. In addition, the Δ_{33} excitation diagrams were also evaluated. The calculations results presented bellow are obtained by coherent summation of IA, FSR and Δ_{33} excitation diagrams:

$$M = M_{IA} + M_{FSR} + M_{\Delta}. \tag{32}$$

Amplitudes M_{IA}, M_{FSR} and M_{Δ} correspond to the diagrams A, B and C shown in Fig 2.

The spin structure of the input NN amplitudes is included in the energy-dependent phase shift analysis (PSA) of Arndt et al. [47]. Following Everett [48], in the triangle diagram B, the NN amplitudes were taken out of the loop integral, and evaluated at the optimum Fermi momentum. However when the nucleon pair interacting in the final state has a small relative energy, it is necessary and possible to correct this NN amplitude for the off-shell behavior of the intermediate state [49–51]).

$$\mathrm{M}^{off} = \mathrm{M}^{on} \; f(s_{31}, m_v^2) \; , \tag{33}$$

The form factor f is a function of the invariant energy s_{31} of the pair and of the virtual mass ($m_v^2 = e^2 - p^2$) of one of the intermediate nucleon. Its precise form can be derived from the deuteron momentum wave function using closure, as in Ref [52]. This form factor was kept with proper propagators and vertices in the loop integral and replaced by unity above 200 MeV.

The amplitude $M_{\pi d \to NN}$ has been computed taking into account the one-loop diagrams with the $N\Delta_{33}$ as intermediate state and also the diagrams with the πN scattering in the S, P and D waves parameterized by their phase shifts. In order to avoid double counting we have excluded the nucleon pole in the πN amplitude which already contributes to the IA term in (32), and the P_{11} wave in the πN scattering which is part of the FSR term. Finally, the ρ-exchange is also taken into account in the interaction of the two nucleons of the $\pi d \to NN$ amplitude. Further details can be found in [53].

In the framework of this model a very good description of the exclusive unpolarized differential cross sections for the d(p,2p)n reaction studied in Gatchina has been obtained [15]. It should be stressed that here kinematics are developed to include events out of the scattering plane; the calculations are integrated over the experimental aperture of the detectors.

A more complete description of the model is in progress and will be published soon .

B. Discussion

The tensor analyzing power A_{YY} for each setting of the SPES 4 central momentum, and for both high and low energy solutions, is shown in Fig 11 and Fig 12.

Results of the calculations with the deuteron Bonn wave function are also presented in the figures. At the 1.6, 1.7 and 1.8 GeV/c settings, the tensor analyzing power for the high energy solution shows good agreement with IA in the range $0.03 \leq q \leq 0.20$ GeV/c. Above this region, the simple IA fails but is rather well corrected by additional diagrams. The same behavior is observed at the 1.8 GeV/c setting for the low energy solution. At 1.9, 2.0 and 2.05 GeV/c the strong deviation of the measured tensor analyzing power from IA for both low and high T_2 is not explainable by the calculations. However, including second order terms reveals the right trend with respect to the experimental points.

As it follows from eq (9), in IA the experimental A_{YY} divided by the factor $1 - 3q_Y^2$ should scale versus q for the two kinematic solutions and all the SPES 4 settings. However this is by far not the case, which means unambigously that the IA fails to describe the data at q larger than 0.2 Gev/c, and no modification of the deuteron wave function can help.

The vector analyzing power results are presented in Fig 13 and Fig 14. They exhibit a similar tendency: the full calculations result in a significant correction to the IA above 0.25 GeV/c. A good agreement between the full calculations and the experimental points is achieved at 2.0 and 2.05 GeV/c both for the high and low energy solutions.

Polarization of the forward-scattered protons P_0 and depolarization D_v are presented averaged over each SPES 4 setting in Fig 15 to Fig 18.

A good description is obtained for P_0 when all diagrams are included, whereas it is not the case for D_v. Especially the rather high value of D_v at 220 MeV/c is not reproduced, but the correction to the IA looks reasonable at high q momenta. The IA is closer to the data than the full calculations for the low energy branch especially for intermediate values of q. However, considering the large error bars in this kinematics, it appears that there is no decisive discrimination from the calculations.

V. CONCLUSION

An extensive and consistent set of data on polarization observables has been obtained for the $\vec{d}(p, \vec{p}p)n$ 3-body breakup of deuteron on hydrogen up to deuteron internal momenta $q \simeq 440$ MeV/c.

The vector A_Y and the tensor A_{YY} analyzing powers exhibit a large deviation from IA for internal momenta q larger than 200 MeV/c. The analyzing powers, being ratios of reaction amplitudes, could be thought to be less modified by distorsions of the IA than cross sections, but this simple consideration appears clearly wrong, at least in the kinematics investigated here.

The deviation from the IA is particularly large for the tensor analyzing power. One can conclude, based on tensor analyzing power data only that IA fails to describe the A_{YY} data above 200 MeV/c. This conclusion cannot be changed by means of modification of the deuteron wave function. Description of the data is considerably improved at moderate q when conventional second order terms are included in the reaction mechanism in the framework of the theoretical model discussed above. Noticeable deviations of the theory from the data take place for A_{YY} at large q, where the rescattering (FSR), though showing the right trend, is not sufficient to describe the experimental data for the high energy kinematics branch.

Smaller deviations from IA are found for the vector analyzing power than for A_{YY}. A very good description of theA_Y data has been obtained for all settings of the spectrometer. It should be noted that out of plane scattering is treated and integrated over the experimental acceptance in the calculations.

The excitation of a virtual Δ is found to have very little effect, even though the invariant energy of the nucleon pairs is sometimes very close to $M_N + M_\Delta$. However, it should be mentioned that there is one missing graph in the model; the Δ formation on the target proton.

The polarization P_0 of the fast proton measured for the high energy branch is convincingly reproduced by the model. This is a good test for the understanding of the reaction mechanism, because this observable is not sensitive in first order to the deuteron structure. The depolarization parameter D_v is poorly reproduced by the model.

To conclude , the polarisation data obtained in this experiment have provided a severe test of a detailed model of the $\vec{d}p \to \vec{p}pn$ reaction mechanism around1 GeV per nucleon.

The model has been already successfully used for description of the Gatchina unpolarized exclusive breakup data [15]. Importance of corrections to the IA in various kinematic conditions is clearly demonstrated both by polarized and unpolarized exclusive experiments. However it does not give a coherent and precise picture of all observables.

Nevertheless we do not have much freedom to use very different deuteron wave functions, taking into consideration the good description of the unpolarized deuteron break-up data obtained in the framework of the same model.

The agreement obtained between data (especially A_Y) and theory with a conventional deuteron wave function implies that new degrees of freedom in the deuteron structure, like six quark bag, are not revealed in the kinematic region investigated.

VI. ACKNOWLEDGMENTS

The authors wish to thank the SATURNE staff for the quality of the polarized deuteron beam provided during the experiment and for the management of the liquid hydrogen target.

We are grateful to M. Rouger for the conception and management of various parts of the electronics, subsequently taken in charge with great efficiency by J.P. Mouly. The management of many pieces of equipment for the experiment, especially the R.S. detectors was efficiently insured by J.C. Lugol, J. Habault and J. le Meur.

We would like also to acknowledge M. Strikman, L. Frankfurt and J.M. Laget for fruitful theoretical discussions.

---

[1] G. Alberi, L.P. Rosa, and Z.D. Thomé, Phys. Rev. Lett. **34**, 503 (1975).

[2] T.E.O. Erikson and M. Rosa-Clot, Ann. Rev. Nucl. Sci. **35**, 271 (1985).

[3] M.I. Strikman and L.L. Frankfurt, Nucl. Phys. **A405**, 557 (1983).

[4] R. Machleidt, K. Holinde, and Ch. Elster, Phys. Pep. **149**, 2 (1987).

[5] M. Lacombe, B. Loiseau, R. Vinh Mau, J. Côté, P. Pirés, and R. de Tourreil, Phys. Lett. **101B**, 139 (1981).

[6] M. Garçon, J. Arvieux, D. H. Beck, E.J. Beise, A. Boudard, E.B. Cairns, J.M. Cameron, G.W. Dodson, K.A. Dow, M. Farkhondeh, H.W. Fielding, J.B. Flanz, R. Goloskie, S. Høibråten, J. Jourdan, S. Kowalski, C. Lapointe, W.J. McDonald, B. Ni, L.D. Pham, R.P. Redwine, N.L. Rodning, G. Roy, M.E. Schulze, P.A. Souder, J. Soukup, I. The, W.E. Turchinetz, C.F. Williamson, K.E. Wilson, S.A. Wood, and W. Ziegler, Phys. Rev. **C 49**, 2516 (1994).

[7] C.F. Perdrisat, L.W. Swenson, P.C. Gugelot, E.T. Boschitz, W.K. Roberts, J.S. Vincent, and J.R. Priest, Phys. Rev. **187**, 1201 (1969).

[8] T.R. Witten, M. Furic, G.S. Mutchler, C.R. Fletcher, N.D. Gabitzsch, G.C. Phillips, J. Hudomalj, L.Y. Lee, B.W. Mayes, J. Allred, and C. Goodman, Nucl. Phys. **A254**, 269 (1975).

[9] R.D. Felder, T.R. Witten, T.M. Williams, M. Furic, G.S. Mutchler, N.D. Gabitzsch, J. Hudomalj-Gabitzsch, J.M. Clement, Jr. and G.C. Phillips, E.V. Hungerford, L.Y. Lee, M. Warneke, B.W. Mayes, and J.C. Allred, Nucl. Phys. **A264**, 397 (1976).

[10] C.F. Perdrisat, V. Punjabi, M.B. Epstein, D.J. Margaziotis, A. Bracco, H.P. Gubler, W.P. Lee, P.R. Poffenberger, W.T.H. Van Oers, H. Postma, H.J. Sebel, and A.W. Stetz, Phys. Lett. **156B**, 38 (1985).

[11] V. Punjabi, C.F. Perdrisat, W.T.H. Van Oers, P.R. Poffenberger, W.P. Lee, C.A. Davis, A. Bracco, D.J. Margaziotis, J.P. Huber, M.B. Epstein, H. Postma, H.J. Sebel, and A.W. Stetz, Phys. Lett. **179B**, 38 (1986).

[12] V. Punjabi, K.A. Aniol, A. Bracco, C.A. Davis, M.B. Epstein, H.P. Gubler, J.P. Huber, W.P. Lee, D.J. Margaziotis, C.F. Perdrisat, P.R. Poffenberger, H. Postma, H.J. Sebel, A.W. Stetz, and W.T.H. Van Oers, Phys. Rev. **C38**, 2728 (1988).

[13] N.P. Aleshin, S.L. Belostotsky, Yu.V. Dotsenko, O.G. Grebenyuk, L.M. Kochenda, L.G. Kudin, N.P. Kuropatkin, S.I. Manaenkov, O.V. Miklukho, V.N. Nikulin, O.E. Prokofiev, A.Yu. Tsaregorotsev, S.S. Volkov, J. Eró, J. Kecskeméti, P. Koncs, Zs. Kovács, and Z. Seres, Phys. Lett. **237B**, 29 (1990).
[14] M.B. Epstein, J.P. Huber, K.A. Aniol, A. Bracco, C.A. Davis, H.P. Gubler, W.P. Lee, D.J. Margaziotis, C.F. Perdrisat, P.R. Poffenberger, H. Postma, V. Punjabi, H.J. Sebel, A.W. Stetz, and W.T.H. Van Oers, Phys. Rev. **C42**, 510 (1990).
[15] N.P. Aleshin, S.L. Belostotsky, O.G. Grebenyuk, V.A. Gordeev, E.N. Komarov, L M. Kochenda, V.I. Lasarev, S.I. Manaenkov, O.V. Miklukho, V.V. Nelyubin, V.N. Nikulin, O.E. Prokofiev, V.V. Sulimov, V.V. Vikhrov, A. Boudard and J.M. Laget, Nucl. Phys. **A568**, 809 (1994).
[16] R.G. Arnold, B.T. Chertok, E.B. Dally, A. Grigorian, C.L. Jordan, W.P. Schütz, R. Zdaarko, F. Martin, and B. A. Mecking, Phys. Rev. Lett. **35**, 776 (1975).
[17] W.P. Schütz, R.G. Arnold, B.T. Chertok, E.B. Dally, A. Grigorian, C.L. Jordan, R. Zdaarko, F. Martin, and B.A. Mecking, Phys. Rev. Lett. **38**, 259 (1977).
[18] M. Bernheim, A. Bussière, J. Mougey, D. Royer, D. Tarnowski, S. Turck-Chieze, S. Frullani, G.P. Capitani, E. de Sanctis, and E. Jans, Nucl. Phys. **A365**, 349 (1981).
[19] L. Anderson, W. Brückner, E. Moeller, S. Nagamia, S. Nissen-Meyer, L. Schroeder, G. Shapiro, and H. Steiner, Phys.Rev. **C28**, 1224 (1983).
[20] V.G. Ableev, D.A. Abdushukurov, S.A. Avramenko, Ch. Dimitrov, A. Filipkowski, A.P. Kobushkin, D.K. Nikitin, A.A. Nomofilov, N.M. Piskunov, V.I. Sharov, I.M. Sitnik, E.A. Strokovsky, L.N. Strunov, L. Viziereva, G.G. Vorobiev, and S.A. Zaporozhets , Nucl. Phys. **A393**, 491 (1983).
[21] C.F. Perdrisat, V. Punjabi, C. Lyndon, J. Yonnet, R. Beurtey, M. Boivin, A. Boudard, J.P. Didelez, R. Frascaria, T. Reposeur, R. Siebert, E. Warde, F. Plouin, P.C. Gugelot, and J.Y. Grossiord, Phys. Rev. Lett. **59**, 2840 (1987).
[22] V. Punjabi, C.F. Perdrisat, P. Ulmer, C. Lyndon, J. Yonnet, R. Beurtey, M. Boivin, F. Plouin, J.P. Didelez, R. Frascaria, T. Reposeur, R. Siebert, E. Warde, A. Boudard, and P.C. Gugelot, Phys. Rev. **C39**, 608 (1989).
[23] S.I. Mishnev, D.M. Nikolenko, S.G. Popov, I.A. Rachek, A.B. Temnykh, D.K. Toporkov, E.P. Tsentalovich, B.B. Wojtsekhowski, S.L. Belostotsky, V.V. Nelyubin, V.V. Sulimov, and V.N. Stibnov, Phys. Lett. **B302**, 23 (1993).
[24] E. Passchier: Thesis Universiteit Utrecht (1996) ISBN 90-393-1243-5.
[25] V.G. Ableev, L. Visireva, V.I. Volkov, S.V. Dzhmukhadze, S.A. Zaporozhets, A.D. Kirillov, A.P. Kobushkin, V.I. Kotov, B. Kuehn, P.K. Many'akov, V.A. Monchinskii, B. Naumann, L. Naumann, S.A. Novikov, W. Neubert, A.A. Nomofilov, L. Penchev, Yu.K. Pilipenko, N.M. Piskunov, P.A. Rukoyatkin, A.L. Svetov, I.M. Sitnik, E.A. Strokovsky, L.N. Strunov, S.V. Fedukov, V.V. Fimushkin, and V.I. Sharov, Pis'ma ZETF **47**, 558 (1998), [JETP Lett. **47**, 649 (1988)]
[26] E. Cheung, C.F. Perdrisat, K. Beard, J. Yonnet, M. Boivin, R. Beurtey, F. Plouin, V. Punjabi, R. Siebert, R. Frascaria, E. Warde, R. Abegg, W.T.H. van Oers, W.W. Jacobs, S. Nanda, C. Lippert, and P.C. Gugelot, Phys. Lett **B284**, 210 (1992).
[27] A.A. Nomofilov, V.V. Perelygin, V.F. Peresedov, A.E. Senner, V.I. Sharov, V.N. Sotnikov, L.N. Strunov, A.V. Zarubin, L.S. Zolin, S.L. Belostotsky, A.A. Izotov, V.V. Nelyubin, V.V. Sulimov, V.V. Vikhrov, T. Dzikowski, and A. Korejwo, Phys. Lett. **B325**, 327 (1994).
[28] B. Kuehn, V.P. Ladygin, P.K. Many'akov, N.M. Piskunov, I.M. Sitnik, E.A. Strokovsky, L. Penchev, and A.P. Kobushkin, Phys. Lett **B334**, 298 (1994)
[29] L.S. Kisslinger and A.K. Kerman, Phys. Rev. **180**, 1483 (1969).
[30] Yu.M. Tchuvil'sky and Yu.F. Smirnov, J. Phys. G:Nucl. Phys. **4**, 1483 (1978).
[31] A.P. Kobushkin and L. Viziereva, J. Phys. G:Nucl. Phys. **8**, 893 (1982).
[32] V.A. Matveev and P. Sorba, Lett. Nuov. Cim. **20**, 435 (1977).
[33] C.F. Perdrisat and V. Punjabi, Phys. Rev. **C 42**, 1899 (1990).
[34] A.F. Yano , Phys. Lett. **156B**, 33 (1985).
[35] J. Erö, Z. Fodor, P. Koncz, Z. Seres, C.F. Perdrisat, V. Punjabi, A. Boudard, B. Bonin, M. Garçon, R. Lombard, B. Mayer, Y. Terrien, E. Tomasi, M. Boivin, J. Yonnet, H.C. Bhang, M. Youn, S.L. Belostotsky, O.G. Grebenyuk, V.N. Nikulin, and L.G. Kudin, Phys. Rev. **C50**, 2687 (1994).
[36] H.H. Barschall and W. Haeberli ed., Polarization Phenomena in Nuclear Reactions, Madison (1970).
[37] C. Wilkin, Proc. Journées d'étude Saturne, Roscoff, Laboratoire National Saturne report (1979).
[38] V. Punjabi, C.F. Perdrisat, E. Cheung, J. Yonnet, M. Boivin, E. Tomasi-Gustafsson, R. Siebert, R. Frascaria, E. Warde, S.L. Belostotsky, O.V. Miklukho, V.V. Sulimov, R. Abegg, and D.R. Lehman, Phys. Rev. **C46**, 984 (1992).
[39] E. Grorud, J.L. Laclare, A. Ropert, A. Tkatchenko, J. Banaigs, and M. Boivin, NIM **188**, 549 (1981).
[40] J. Arvieux, S.D. Baker, R. Beurtey, M. Boivin, J.M. Cameron, T. Hasegawa, D. Hutcheon, J. Banaigs, J. Berger, E. Codino, J. Dufflo, L. Goldzahl, F. Plouin, A. Boudard, J. Gaillard, Nguyin van Sen, and Ch.F. Perdrisat, Nucl. Phys. **A431**, 613 (1984)
[41] J. Arvieux, S. D. Baker, A. Boudard, J. Cameron, T. Hasegawa, D. Hutcheon, C. Kerboul, G. Gaillard, and Nguen Van Sen , NIM **A273**, 48 (1988).
[42] E. Tomasi-Gustafsson *et al.*, Internal Report LNS/Ph/91-27, L.N.Saturne (1991).
[43] M. Bedjidian, C. Contardo, E. Descroix, S. Gardien, J.Y. Grossiord, A. Guichard, M. Gusakow, R. Haroutunian, M. Jacquin, J.R. Pizzi, D. Bachelier, J.L. Boyard, T. Hennino, J.C. Jourdin, M. Roy-Stephan, and P. Radvanyi, NIM **A257**, 132 (1987)

[44] B. Bonin, A. Boudard, H. Fanet, R.W. Fergerson, M. Garçon, C. Giorgetti, J. Habault, J. le Meur, R.M. Lombard, J.C. Lugol, B. Mayer, J.P. Mouly, E. Tomasi-Gustafsson, J.C. Duchazeaubeneix, J. Yonnet, M. Morlet, J. Van de Wiele, A. Willis, G. Greeniaus, G. Gaillard, P. Markowitz, C.F. Perdrisat, R. Abegg, and D.A. Hutcheon, NIM **A288**, 379 (1990).
[45] M. Youn, *Doctoral thesis*, Seoul National University, Korea, (1993).
[46] R.W. Fergerson, *Doctoral thesis*, LA–16554–T Los Alamos, USA (1985).
[47] R.A. Arndt, J.S. Hyslop, and L.D. Roper, Phys. Rev. **D35**, 128 (1987).
[48] A. Everett, Phys. Rev. **126**, 831 (1962).
[49] B.S. Aladashvili, J-F Germond, V.V. Glagolev, M.S. Nioradze, T. Siemiarczuk, J. Stepaniak, V.N. Streltsov, C. Wilkin, and P. Zieliński, J. Phys. G:Nucl. Phys. **3**, 7 (1977).
[50] C. Alvear and C. Wilkin, J. Phys. G:Nucl. Phys. **10**, 1025 (1984).
[51] V.G. Ksenzov and V.M. Kolybasov, Sov. J. Nucl. Phys. **22**, 372 (1976).
[52] J.M. Laget, Nucl. Phys. **A296**, 389 (1978).
[53] J.M. Laget, Nucl. Phys. **A370**, 491 (1981).

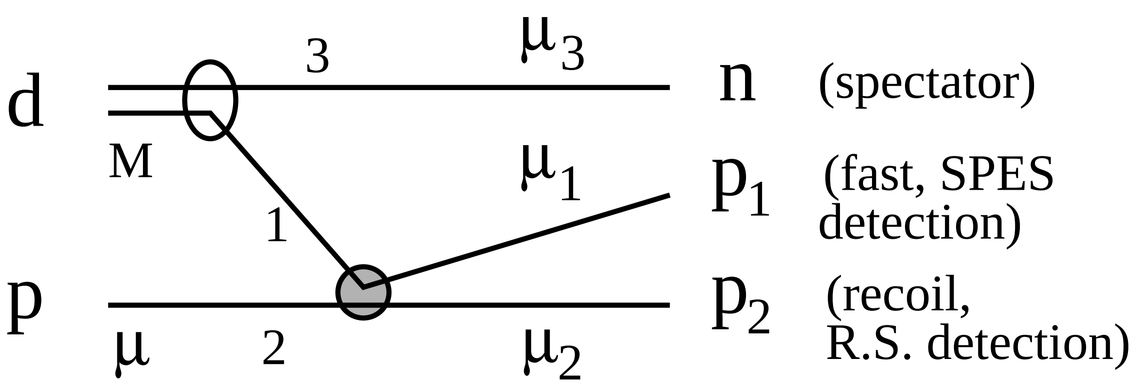

FIG. 1. Notations for the $p(d,2p)n$ reaction. The letters M, μ and μ_i refer to the spin magnetic quantum number of each particle.

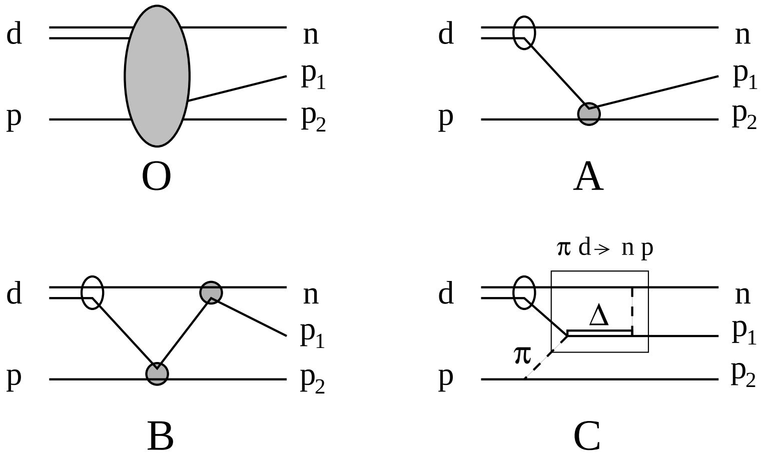

FIG. 2. The Feynman diagrams included into the calculation. The exclusive breakup (O) is the coherent sum of first order impulse approximation (A), final state rescattering (B) and Δ excitation (C). For graphs A and B, the two circular permutations of the final particles are also computed. For graph C, only the permutation of n and p_1 is considered.

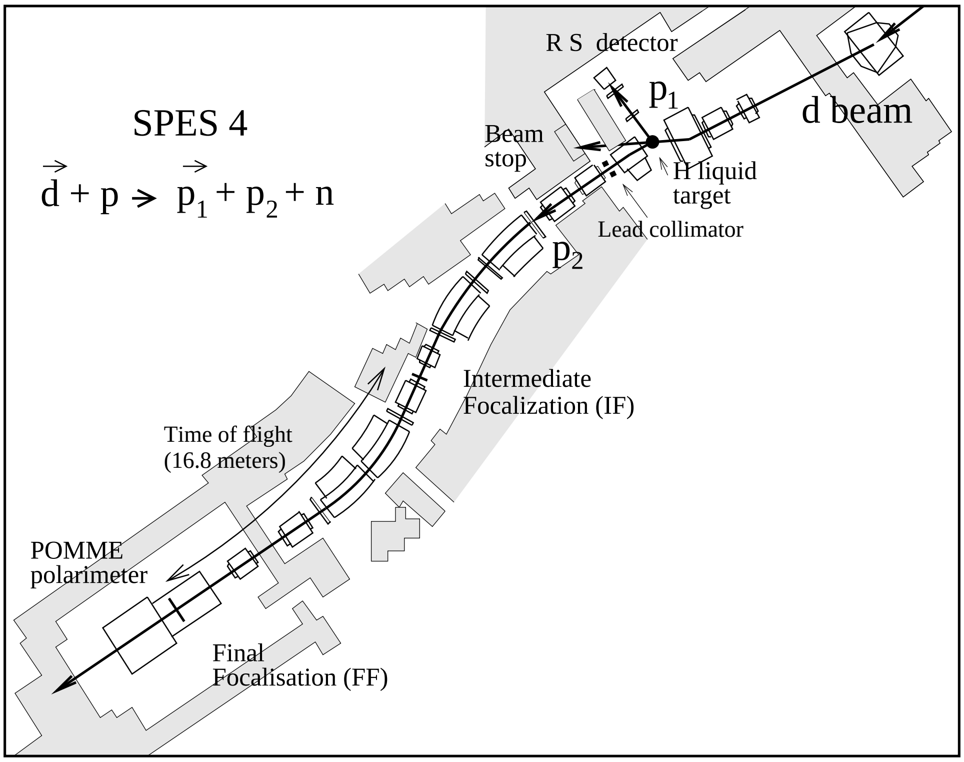

FIG. 3. Experimental setup: The magnets of the beam line and of the SPES 4 spectrometer are shown with the location of the RS arm and of the POMME polarimeter. The shaded areas are concrete walls. The RS detectors are protected from a direct view of the beam stop.

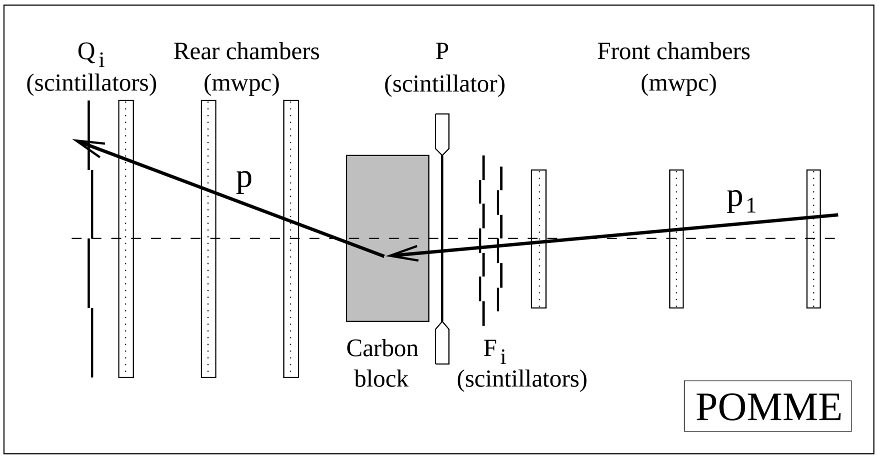

FIG. 4. Polarimeter POMME: The hodoscope of plastic scintillators F_i is located at the final focalization (FF) of the spectrometer. The P and Q_i lath of plastic scintillators are connected to photomultipliers on each side.

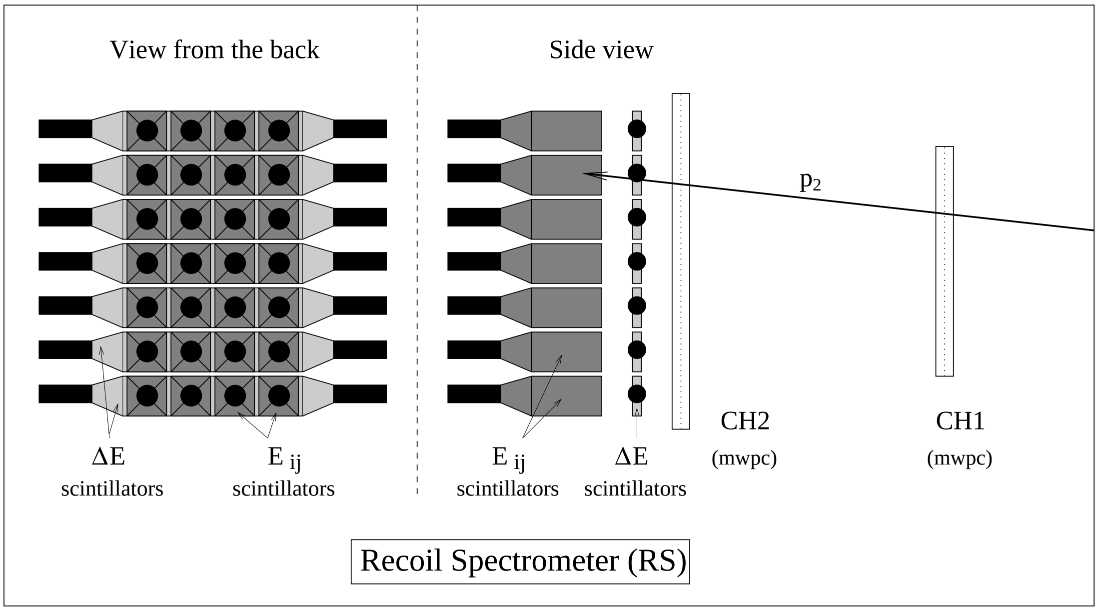

FIG. 5. Recoil Spectrometer (RS): The RS arm is shown from the side (on the right part) and from the back (on the left part). The distance between E_{ij} scintillators and between ΔE scintillators is enlarged on the picture. The distance is actually only the wrapping papers.

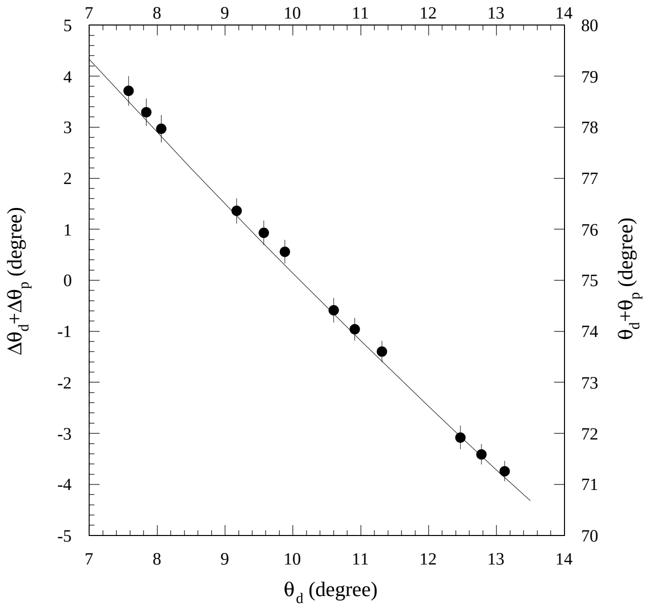

FIG. 6. The correlation from elastic dp scattering data used for calibration.

FIG. 7. The correlation to select the contaminations from background. We used the events inside the contour shown to estimate the contribution from the background.

FIG. 8. The estimated background (a) and real events(b)

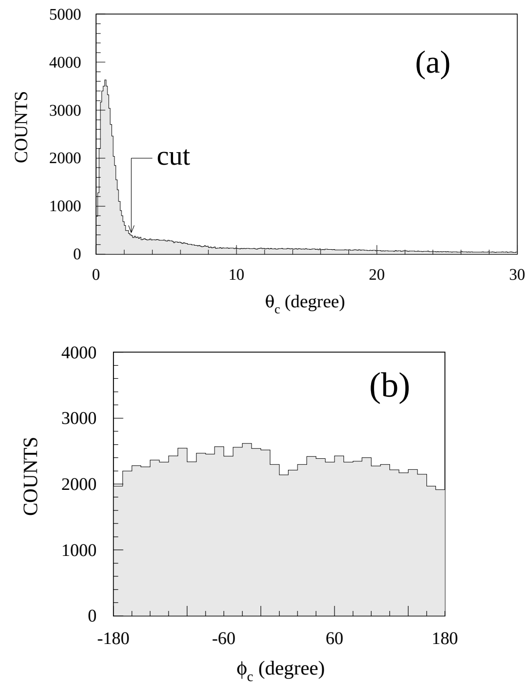

FIG. 9. (a) The distribution of the scattering angle(θ_c) after vertex cut. We used only the events $\theta_c \geq 2.5°$ for the polarization analysis. (b) The final distribution of the azimuthal angle φ_c.

FIG. 10. Depolarization (D_v) of the $\vec{d}+p \rightarrow \vec{p}_1 + p_2 + n$ reaction and polarization (P_0) of the fast proton (p_1) as a function of q, the momentum of the neutron in the deuteron rest frame. Each family of symbol is for a given central momentum p1 detected in SPES 4, the top figures (a) and (c) for the low energy solution of the second proton (p_2) detected in R.S. and the bottom figures (b) and (d) for the high energy one. The binning in q is 50 MeV/c, but the points at the same q value are slightly displaced to see the various error bars.

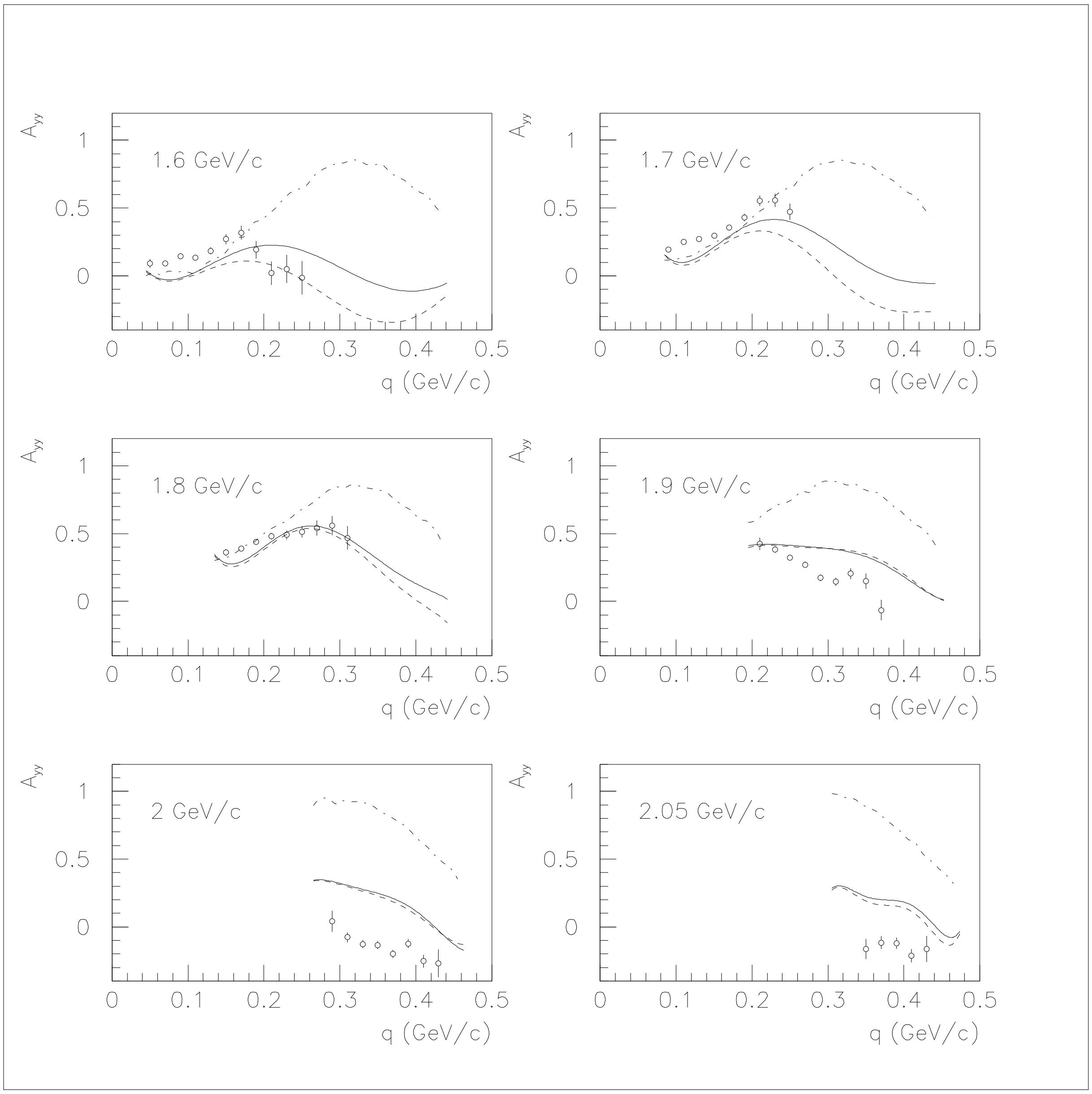

FIG. 11. The tensor analyzing power A_{YY} for high-energy solution. The experimental points are presented for the different values of the central momentum detected in the magnetic spectrometer and as a function of the outgoing neutron momentum expressed in the deuteron rest frame. High and low-energy solution refers to the energy of the slow proton detected at the same angle in R.S. The curves are the calculations explained in the text. The dashed-dotted line is the impulse approximation, the dashed line has in addition the FSR contribution, and the continuous line is the full calculation including in addition the virtual Δ.

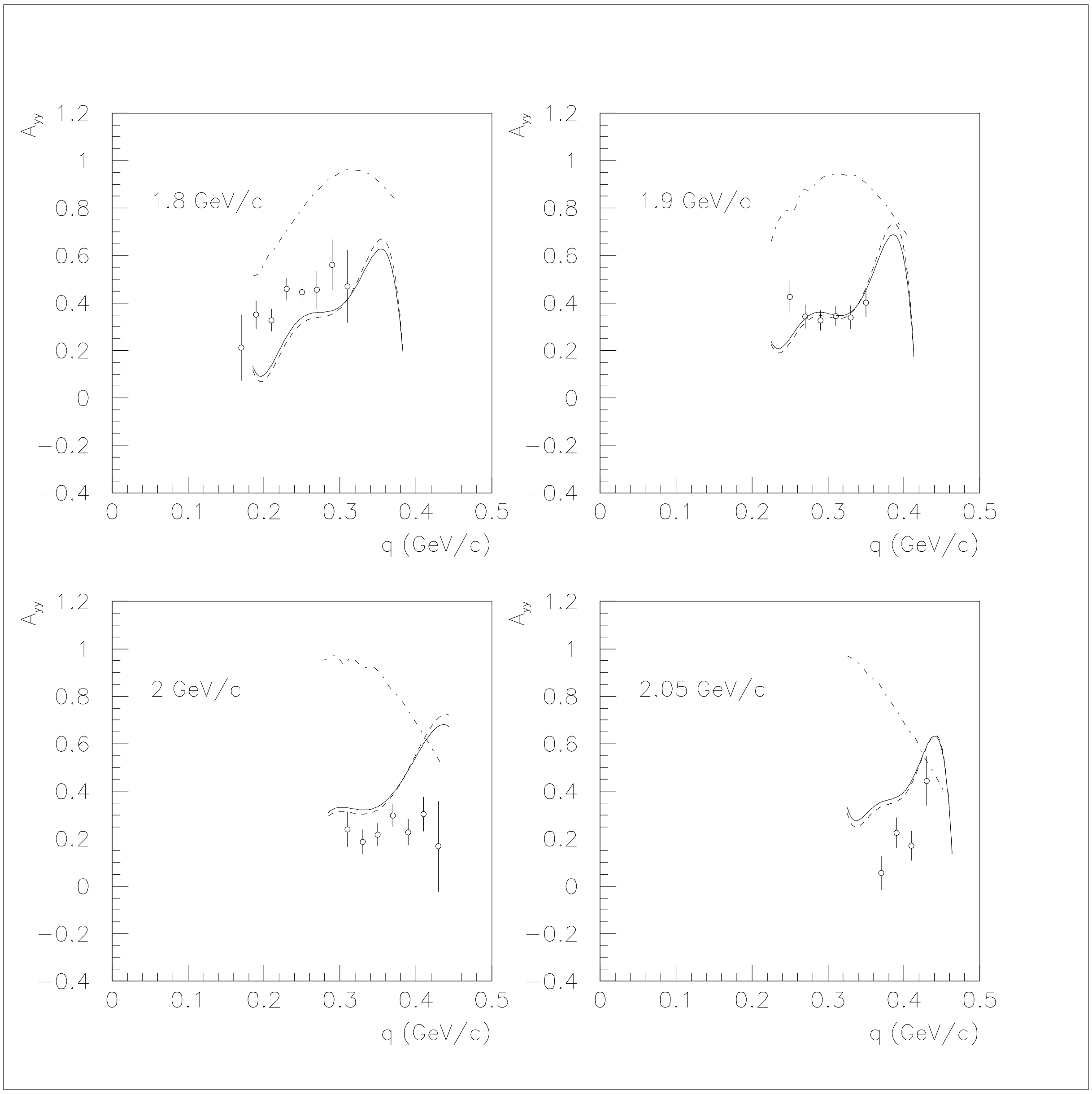

FIG. 12. The tensor analyzing power A_{YY} for low-energy solution. Same notations as in fig 11.

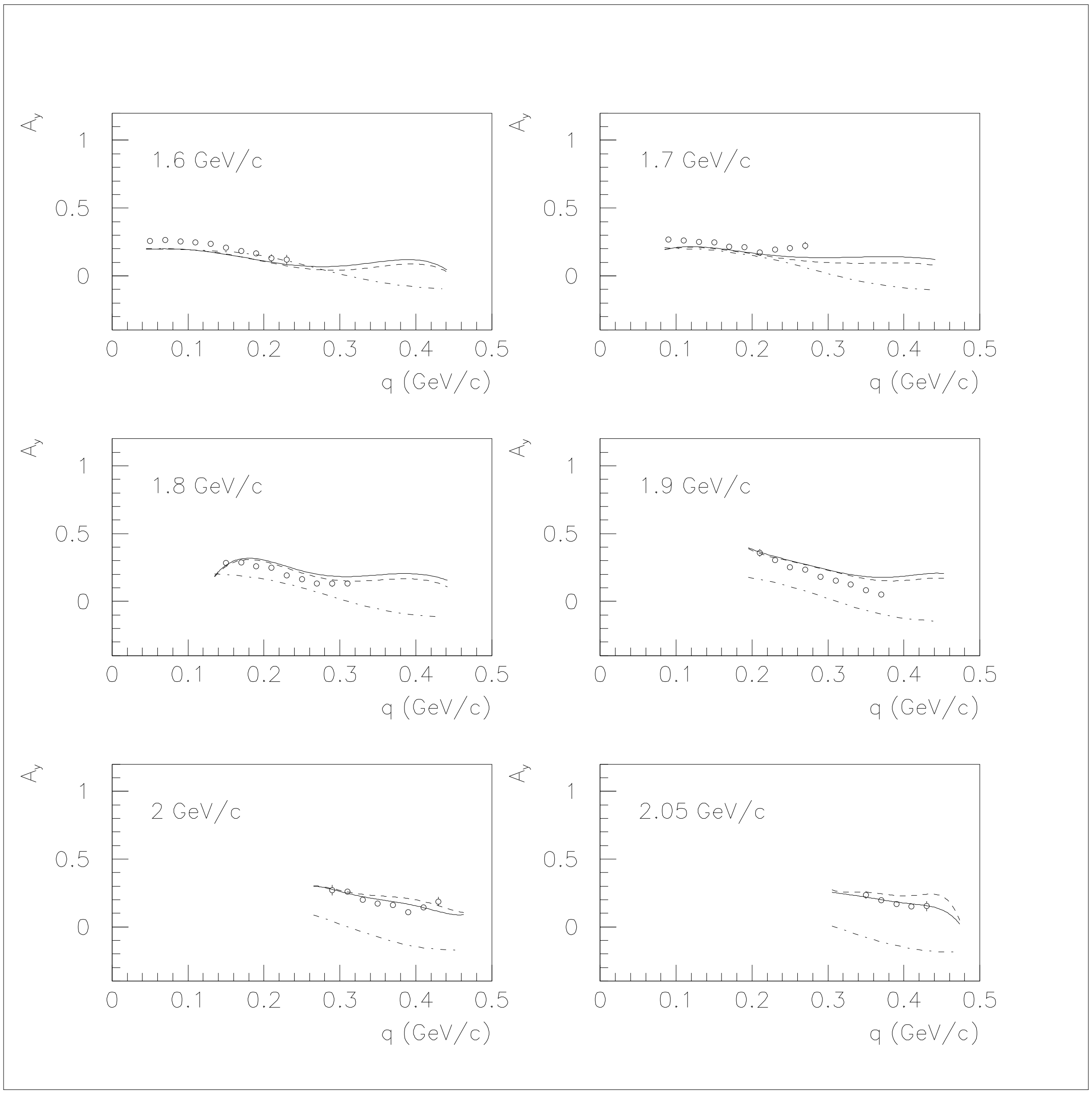

FIG. 13. The vector analyzing power A_Y for high-energy solution. Same notations as in fig 11.

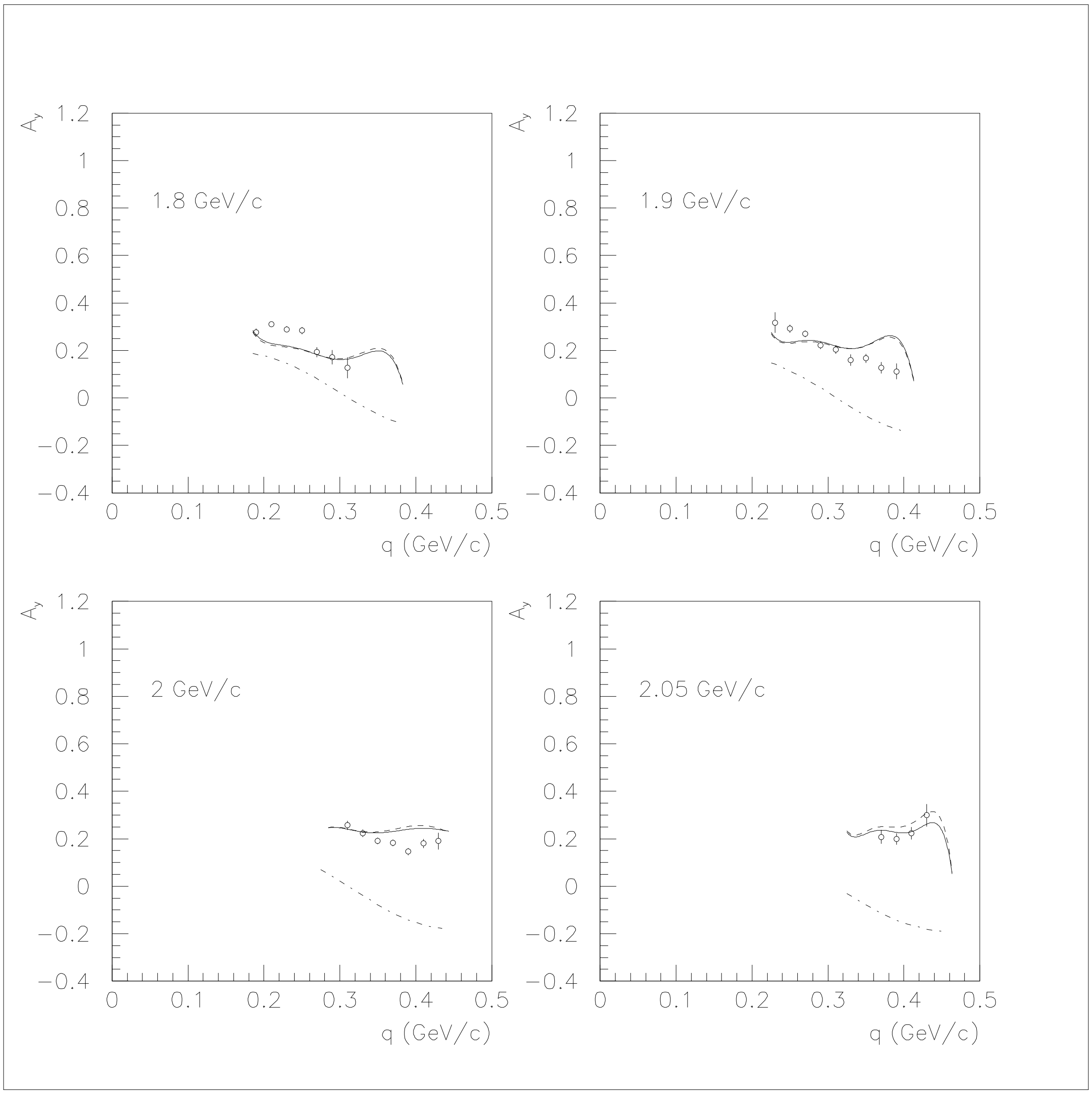

FIG. 14. The vector analyzing power A_Y for low-energy solution. Same notations as in fig 11.

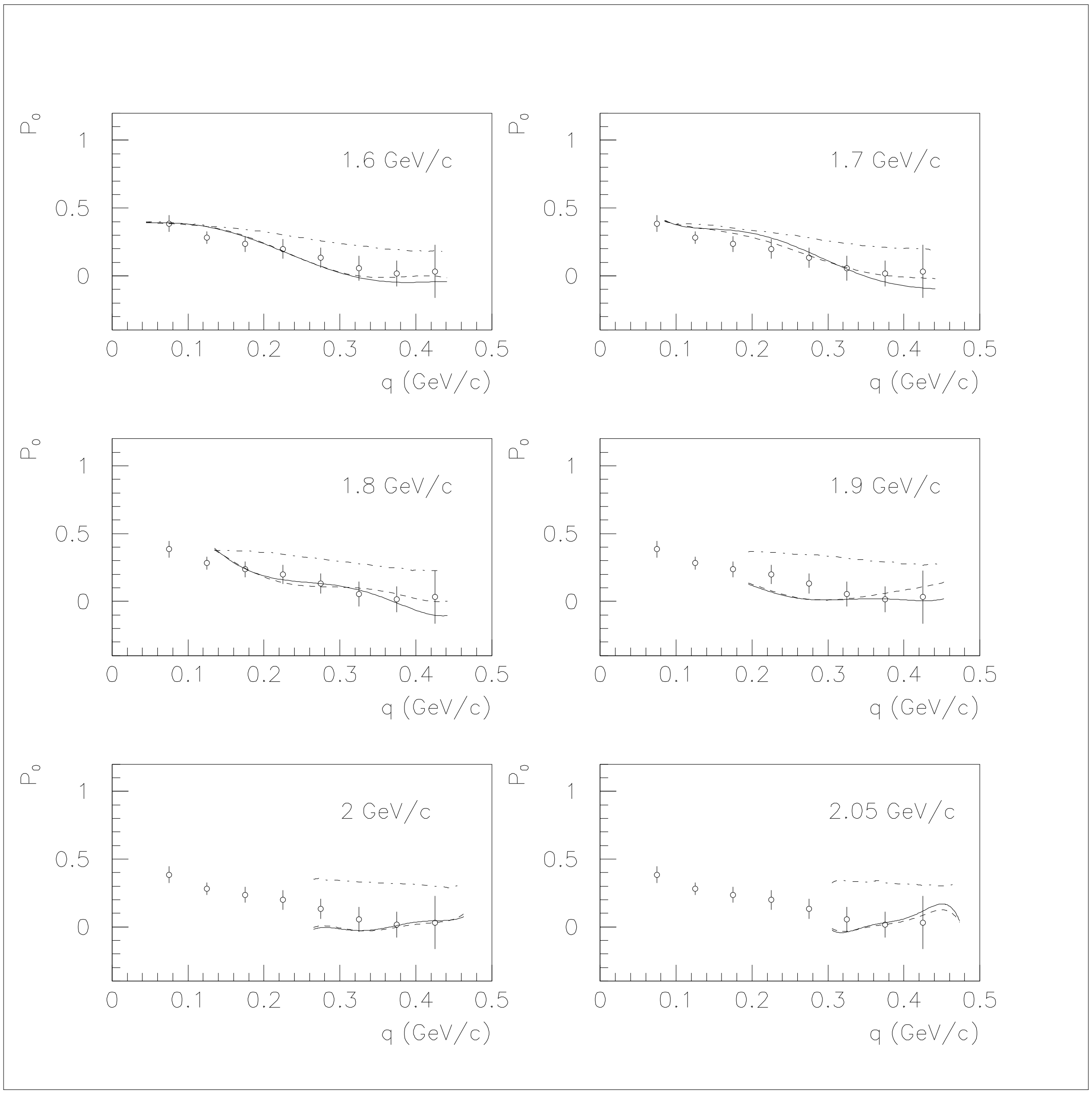

FIG. 15. The forward proton polarization P_0 for high-energy solution. The notation of the curves are the same as in fig 11. The calculations are done consistently as for A_Y and A_{YY} for each setting of the spectrometer while the data are summed as explained in the text.

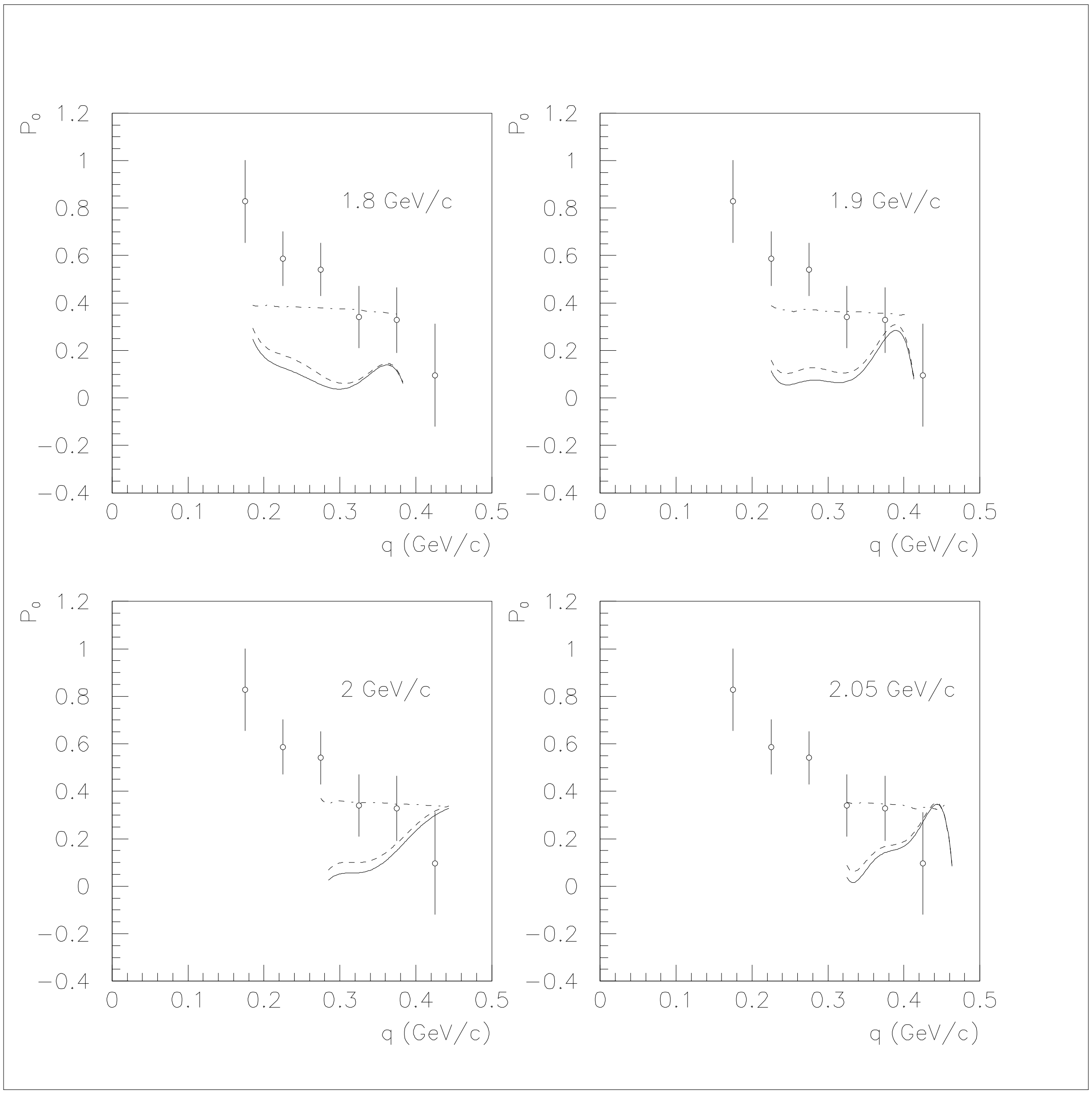

FIG. 16. The forward proton polarization P_0 for low-energy solution. The notation of the curves are the same as in fig 11.

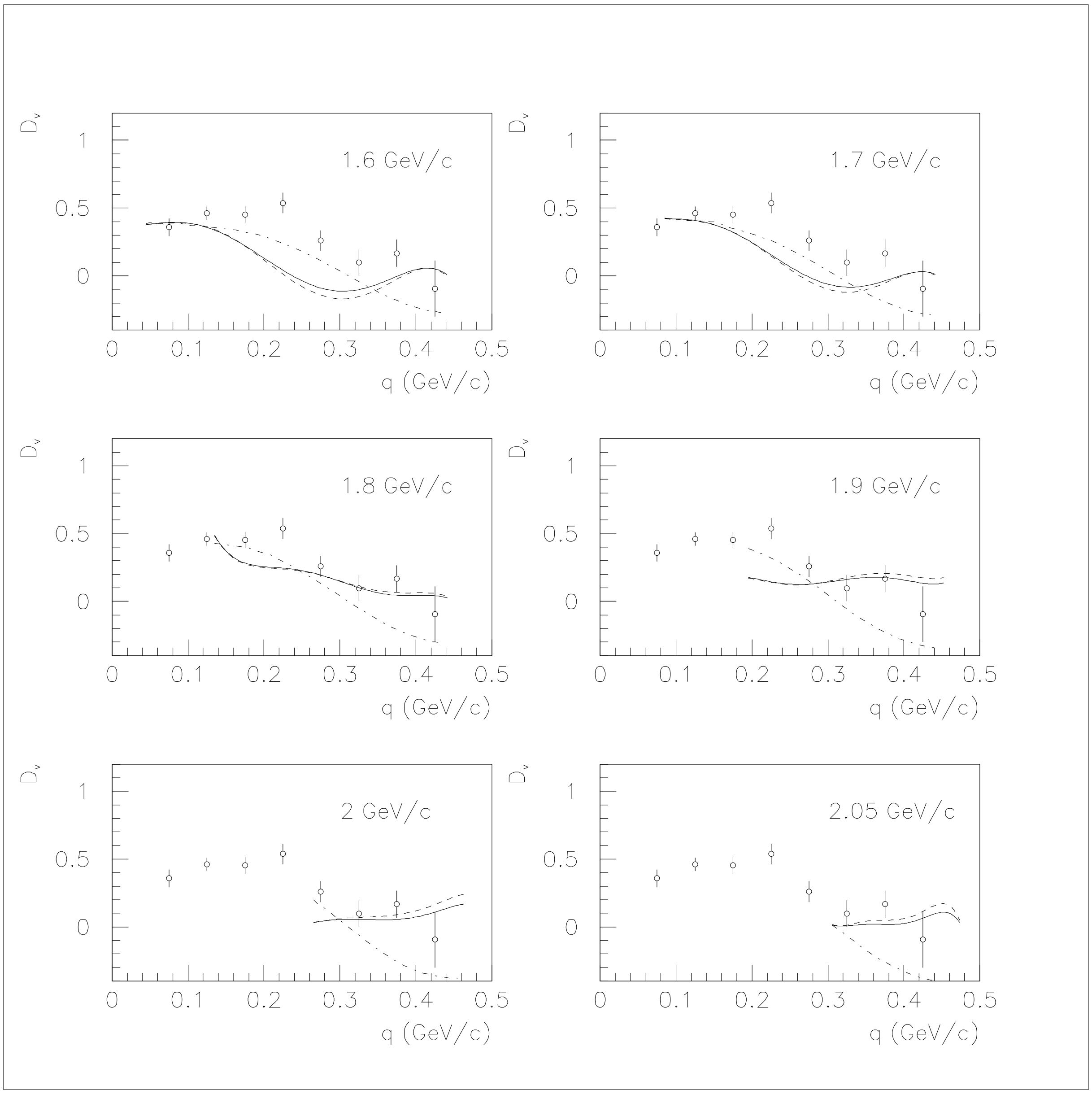

FIG. 17. The depolarization parameter D_v for high-energy solution. Same notations as in fig 11.

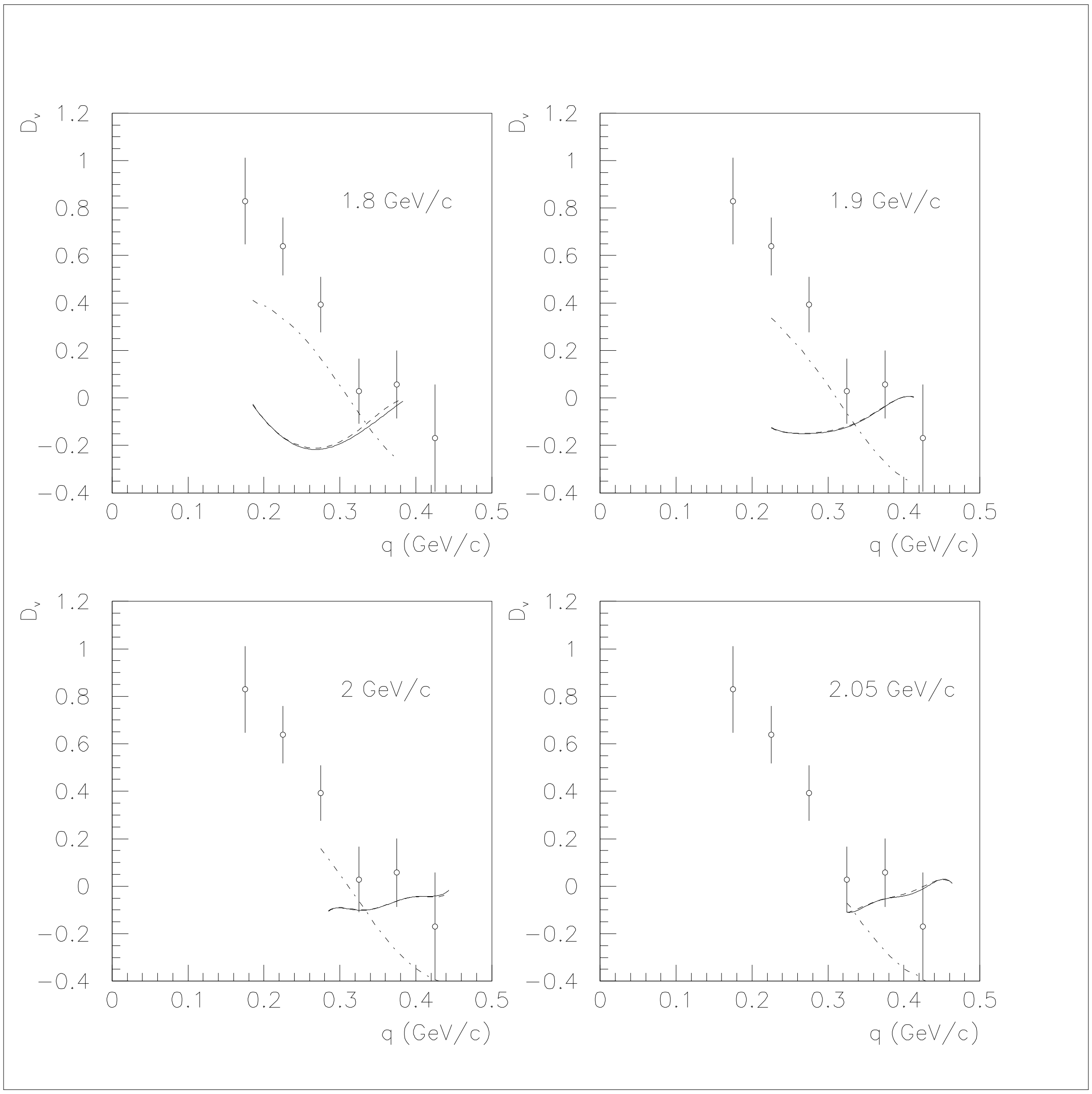

FIG. 18. The depolarization parameter D_v for low-energy solution. Same notations as in fig 11.

TABLE I. Beam polarization extremal value (on the target) and associated beam state number.

assigned beam state number	p_{yy} ; tensor polarization	p_y ; vector polarization
1	0.0	0.0
2	0.0	2/3
3	0.0	-2/3
4	0.0	0.0
5	1.	-1/3
6	1.	1/3
7	-1.	-1/3
8	-1.	1/3

TABLE II. Absolute value of the beam polarization measured during the two runs with the statistical error.

	Run 1	Run 2
p_y (states 2-3)	0.647 ± 0.020	0.633 ± 0.007
p_y (states 5-6-7-8)	0.301 ± 0.017	0.326 ± 0.012
p_{yy}	0.947 ± 0.018	0.912 ± 0.014

TABLE III. Internal momenta q for different SPES 4 settings

p_{10}, GeV/c	q, GeV/c
1.6	0.03 - 0.20
1.7	0.04 - 0.22
1.8	0.10 - 0.38
1.9	0.16 - 0.41
2.0	0.22 - 0.44
2.05	0.29 - 0.45

TABLE IV. Measured values of the tensor and vector analyzing power and statistical (rms) errors as a function of q . See text for details and systematic errors. This table is for the recoiling proton $p2$ of **highest energy**. The momentum p_1 of the fast proton in the laboratory is specified.

p_1 (GeV/c)	q (MeV/c)	A_{YY}	$\sigma(A_{YY})$	A_Y	$\sigma(A_Y)$
1.6	50.0	0.092	0.032	0.256	0.009
	70.0	0.093	0.019	0.265	0.005
	90.0	0.145	0.017	0.255	0.005
	110.0	0.135	0.020	0.248	0.006
	130.0	0.184	0.026	0.238	0.007
	150.0	0.270	0.036	0.210	0.011
	170.0	0.318	0.051	0.183	0.015
	190.0	0.192	0.065	0.164	0.021
	210.0	0.021	0.086	0.129	0.028
	230.0	0.050	0.104	0.120	0.036
	250.0	-0.014	0.124		
1.7	90.0	0.194	0.018	0.270	0.006
	110.0	0.251	0.012	0.259	0.004
	130.0	0.271	0.012	0.249	0.004
	150.0	0.295	0.014	0.246	0.005
	170.0	0.357	0.021	0.214	0.007
	190.0	0.430	0.029	0.210	0.010
	210.0	0.553	0.038	0.173	0.014
	230.0	0.557	0.050	0.194	0.018
	250.0	0.472	0.060	0.203	0.022
	270.0			0.221	0.028
1.8	150.0	0.360	0.025	0.285	0.012
	170.0	0.389	0.019	0.287	0.007
	190.0	0.438	0.020	0.258	0.007
	210.0	0.481	0.023	0.248	0.009
	230.0	0.490	0.032	0.192	0.010
	250.0	0.512	0.043	0.164	0.013
	270.0	0.540	0.057	0.131	0.017
	290.0	0.559	0.071	0.130	0.022
	310.0	0.468	0.087	0.132	0.020
1.9	210.0	0.424	0.046	0.358	0.029
	230.0	0.382	0.022	0.304	0.009
	250.0	0.321	0.021	0.251	0.008
	270.0	0.270	0.022	0.234	0.008
	290.0	0.175	0.025	0.180	0.009
	310.0	0.145	0.031	0.154	0.010
	330.0	0.204	0.041	0.124	0.012
	350.0	0.149	0.057	0.083	0.015
	370.0	-0.065	0.076	0.051	0.019
2.0	290.0	0.041	0.077	0.270	0.039
	310.0	-0.076	0.036	0.259	0.011
	330.0	-0.126	0.031	0.201	0.009
	350.0	-0.133	0.029	0.172	0.009
	370.0	-0.200	0.030	0.162	0.009
	390.0	-0.122	0.034	0.110	0.010
	410.0	-0.252	0.047	0.144	0.014
	430.0	-0.268	0.102	0.187	0.033
2.05	350.0	-0.163	0.075	0.237	0.028
	370.0	-0.116	0.047	0.197	0.018
	390.0	-0.121	0.041	0.167	0.017
	410.0	-0.211	0.049	0.151	0.020
	430.0	-0.163	0.094	0.154	0.037

TABLE V. Measured values of the tensor and vector analyzing power and statistical (rms) errors as a function of q . See text for details and systematic errors. This table is for the recoiling proton $p2$ of **lowest energy**. The momentum p_1 of the fast proton in the laboratory is specified.

p_1 (GeV/c)	q (MeV/c)	A_{YY}	$\sigma(A_{YY})$	A_Y	$\sigma(A_Y)$
1.7	150.0			0.293	0.021
	170.0			0.344	0.014
	190.0			0.320	0.016
	210.0			0.281	0.021
	230.0			0.208	0.029
	250.0			0.217	0.050
1.8	170.0	0.211	0.139		
	190.0	0.350	0.059	0.275	0.018
	210.0	0.328	0.047	0.311	0.012
	230.0	0.459	0.048	0.289	0.013
	250.0	0.445	0.057	0.284	0.015
	270.0	0.455	0.079	0.193	0.021
	290.0	0.562	0.106	0.172	0.030
	310.0	0.470	0.153	0.127	0.045
1.9	230.0			0.317	0.044
	250.0	0.426	0.066	0.292	0.017
	270.0	0.343	0.051	0.271	0.014
	290.0	0.327	0.043	0.221	0.015
	310.0	0.345	0.042	0.204	0.018
	330.0	0.339	0.049	0.160	0.025
	350.0	0.400	0.060	0.167	0.019
	370.0			0.127	0.024
	390.0			0.112	0.033
2.0	310.0	0.238	0.075	0.257	0.020
	330.0	0.186	0.052	0.223	0.016
	350.0	0.218	0.049	0.191	0.014
	370.0	0.299	0.049	0.183	0.014
	390.0	0.228	0.056	0.146	0.015
	410.0	0.303	0.073	0.181	0.019
	430.0	0.168	0.191	0.190	0.036
2.05	370.0	0.056	0.072	0.208	0.028
	390.0	0.226	0.065	0.199	0.025
	410.0	0.171	0.063	0.223	0.026
	430.0	0.444	0.104	0.299	0.047